

# Pulsars and Millisecond Pulsars II: Deep diving into the Evolutionary Mechanisms

Maria Rah<sup>1,2,\*</sup>, Rainer Spurzem<sup>2,3,6</sup>, Francesco Flammini Dotti<sup>4,5,3</sup>, Areg Mickaelian<sup>1</sup>

<sup>1</sup> NAS RA V.Ambartsumian Byurakan Astrophysical Observatory (BAO), Byurakan, Armenia

<sup>2</sup> The Silk Road Project at the National Astronomical Observatory, Chinese Academy of Sciences, China

<sup>3</sup> Astronomisches Rechen-Inst., ZAH, Univ. of Heidelberg, Germany

<sup>4</sup> Department of Physics, New York University Abu Dhabi, PO Box 129188 Abu Dhabi, UAE

<sup>5</sup>Center for Astrophysics and Space Science (CASS), New York University Abu Dhabi, PO Box 129188, Abu Dhabi, UAE

<sup>6</sup>Kavli Institute for Astronomy and Astrophysics, Peking University, China

## Abstract

This study investigates the evolutionary spin behaviors, both spin-down and spin-up, of canonical pulsars and millisecond pulsars (MSPs) in the unique dynamical environments of globular clusters, with a particular focus on identifying distinct evolutionary channels that can be modeled using direct  $N$  body simulations (via NBODY6++GPU). Leveraging observational data from the ATNF Pulsar Catalogue, we compile a sample of 80 pulsars divided into four populations: normal and millisecond pulsars in both the Galactic field and globular clusters. Through detailed analysis of pulsar spin periods ( $P$ ) and their derivatives ( $P'$ ), along with derived quantities such as surface magnetic field strength ( $B$ ), rotational energy loss rate ( $E'$ ), and characteristic age ( $\tau_c$ ), we construct a comprehensive  $P$ – $P'$  diagram that captures the physical and evolutionary diversity of these sources. We identify seven distinct evolutionary scenarios that describe the spin evolution of pulsars in globular clusters, including tidal spin-up, exchange interactions, accretion from low-mass companions, magnetic field decay, and triple system evolution. Each scenario outlines a possible formation channel for observed pulsar properties and is suitable for forward modeling using direct  $N$ -body methods coupled with binary stellar evolution recipes. By integrating pulsar observational data with astrophysical modeling requirements, this work lays the foundation for self-consistent simulation frameworks aimed at reproducing observed pulsar populations in dense stellar systems. The results have implications for neutron star retention, recycling pathways, and the long-term dynamical evolution of stellar clusters harboring MSPs.

**Keywords:** *Pulsars, Millisecond Pulsars, Evolution, Spin-Up, Spin-Down, Binary Interactions*

## 1. Introduction

Neutron stars, the remnants of massive stars following supernova explosions, exhibit a diverse range of behaviors and characteristics, with pulsars forming a significant subclass due to their periodic emission of electromagnetic radiation. Pulsars are characterized by their rapid rotation and intense magnetic fields, typically ranging from  $10^{12}$  to  $10^{15}$  Gauss, which drive the emission of beams detectable across multiple wavelengths (Shi & Ng, 2024). Within this broad category, a hierarchical structure emerges on the basis of their rotational properties and evolutionary pathways, as detailed below.

At the top of this hierarchy are normal pulsars, which possess spin periods typically ranging from 0.1 to several seconds. These objects are often isolated or found in environments with minimal dynamical interactions, such as the Galactic field (GF), and their evolution is primarily governed by magnetic dipole radiation leading to spin-down (Han et al., 2021). Normal pulsars represent the majority of the pulsar population, with

\*mariarah.astro@gmail.com, Corresponding author

their numbers significantly outpacing other subclasses, as evidenced by the cumulative discovery trends shown in the first paper in this series (Rah et al., 2024).

A distinct subclass within pulsars is the millisecond pulsars (MSPs), characterized by their exceptionally short spin periods, typically between 1 and 10 milliseconds. MSPs are often the product of a "recycling" process in binary systems, where angular momentum transfer from a companion star accelerates the neutron star's rotation. This process, frequently occurring in low-mass X-ray binaries (LMXBs), not only shortens the spin period but also reduces the magnetic field strength to around  $10^8$  to  $10^9$  Gauss, distinguishing MSPs from their slower counterparts (Chatopadhyay et al., 2021, Demorest et al., 2010). The prevalence of MSPs is notably higher in dense environments like globular clusters (GCs), where binary interactions are more frequent (Hui et al., 2010,?).

Within the MSP population, a further subcategory emerges: transitional millisecond pulsars (tMSPs). These objects are unique in that they alternate between accretion-powered X-ray states and rotation-powered radio states, providing a window into the evolutionary transition between these phases. tMSPs are often found in binary systems and are thought to represent a critical stage in the recycling process, where the pulsar transitions from an active accretion phase to a radio MSP phase. Recent observations, such as those by (Bahramian et al., 2018), have identified several tMSPs in globular clusters, highlighting their role in understanding the recycling mechanism (Galloway & Keek, 2021).

The hierarchical structure of pulsars, MSPs, and tMSPs underscores the complexity of their evolutionary pathways, which are influenced by both intrinsic properties (e.g., magnetic field strength, spin period) and external factors (e.g., environmental density, binary interactions). Theoretical models, such as those developed using NBODY6++GPU, have been instrumental in simulating these evolutionary processes, particularly in dense stellar environments (Spurzem & Kamlah, 2023, and references therein). Additionally, the work of (Hui et al., 2010) and (Hui et al., 2010) provides critical insights into the formation and evolution of MSPs in globular clusters, citing earlier studies like (Belczynski et al., 2016) to emphasize the role of binary interactions in shaping MSP populations.

This paper, the second in a series, builds on the statistical foundation laid in the first paper (Rah et al., 2024) to explore the special evolutionary mechanisms governing pulsars, MSPs, and tMSPs. By integrating recent observational data and advanced theoretical models, we aim to deepen our understanding of the physical processes driving their evolution, with a particular focus on spin-up, spin-down, and the role of binary interactions (Shi & Ng, 2024, Zhang et al., 2023).

## 2. Fundamental Parameters and Key Relations of Pulsars

Understanding the evolution of pulsars requires familiarity with their fundamental parameters and the key relations that govern their behavior. These parameters not only define the physical characteristics of pulsars but also provide insights into their evolutionary stages and the underlying mechanisms driving their rotation and energy loss. Here, we outline the most critical parameters and their associated relations, which serve as the foundation for the subsequent discussion on evolutionary mechanisms. A comprehensive summary of pulsar parameters, categorized by population and environment, is provided in Tables 1, 2, 3, and 4, located at the end of the manuscript.

The primary observable parameter of a pulsar is its spin period,  $P$ , which represents the time taken for one complete rotation, typically ranging from milliseconds to several seconds. For normal pulsars,  $P$  is often between 0.1 and 10 seconds, while millisecond pulsars (MSPs) exhibit much shorter periods, typically between 1 and 10 milliseconds (Lorimer, 2008). Closely related to the spin period is the period derivative,  $\dot{P}$ , which measures the rate of change of the spin period over time (in units of s/s). This parameter quantifies the slow-down of the pulsar's rotation, driven by energy loss mechanisms such as magnetic dipole radiation. For example, the Crab Pulsar (PSR B0531+21) has a period of  $P \approx 33$  ms and a period derivative of  $\dot{P} \approx 4.2 \times 10^{-13}$  s/s, while an MSP like PSR J0437-4715 has  $P \approx 5.75$  ms and  $\dot{P} \approx 5.7 \times 10^{-20}$  s/s (Manchester et al., 2005).

Another crucial parameter is the surface magnetic field strength,  $B$ , which drives the pulsar's emission and energy loss. The magnetic field is typically inferred from the spin period and its derivative using the relation for magnetic dipole radiation:

$$B \approx 3.2 \times 10^{19} \sqrt{PP} \text{ Gauss,}$$

where  $P$  is in seconds and  $\dot{P}$  is in s/s (Lorimer, 2008). This relation assumes that the pulsar's spin-down is primarily due to the emission of magnetic dipole radiation, a reasonable approximation for most isolated pulsars. Normal pulsars typically have magnetic fields in the range of  $10^{12}$  to  $10^{15}$  Gauss, while MSPs, due to the recycling process, have significantly weaker fields, typically between  $10^8$  and  $10^9$  Gauss (Chattopadhyay et al., 2021). The magnetic field strength is a key indicator of the pulsar's evolutionary state, as it influences the rate of energy loss and the pulsar's emission properties across multiple wavelengths.

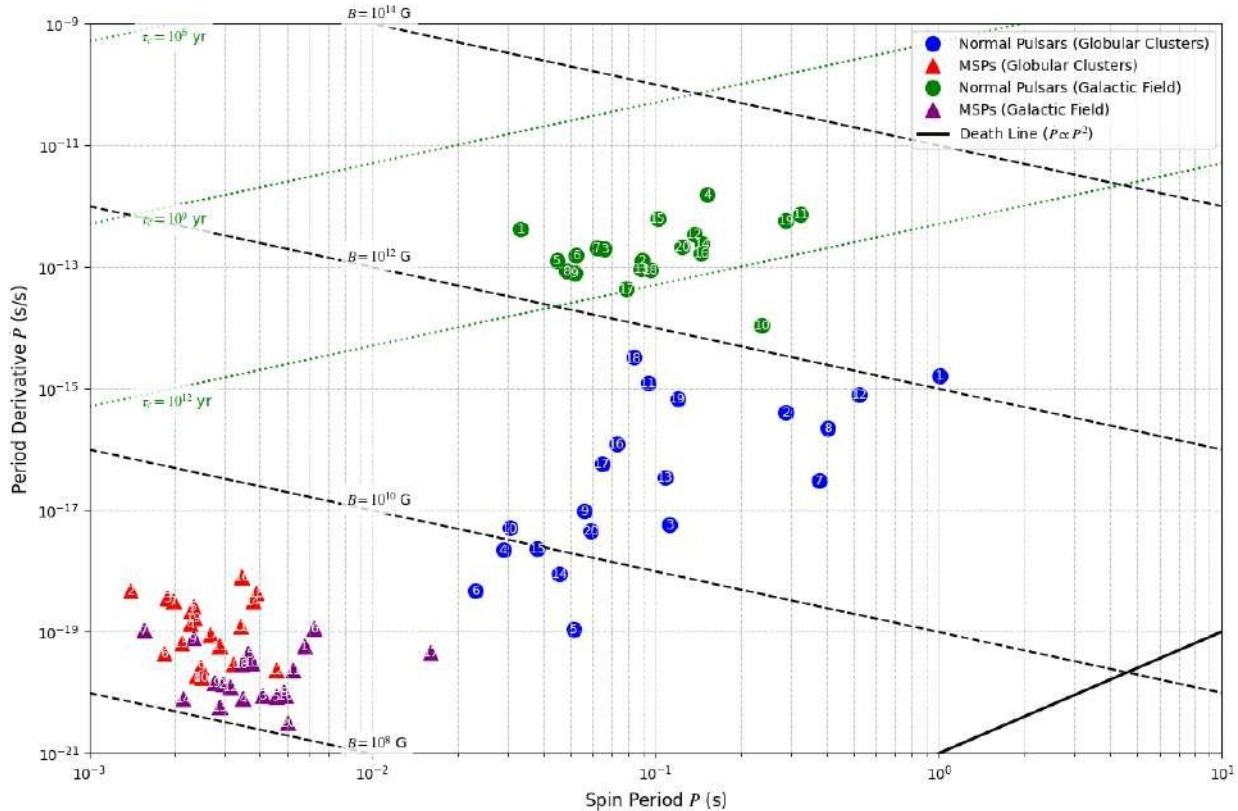


Figure 1.  $P - P'$  diagram illustrating the distribution of four pulsar sub-populations: normal pulsars in globular clusters (blue circles), millisecond pulsars (MSPs) in globular clusters (red triangles), normal pulsars in the Galactic field (green circles), and MSPs in the Galactic field (purple triangles), numbered according to Tables 1, 2, 3, and 4. The x-axis spans spin periods from  $10^{-3}$  to  $10^1$  s, and the y-axis covers period derivatives from  $10^{-21}$  to  $10^{-9}$  s/s, both on logarithmic scales. Dashed green lines indicate characteristic age contours ( $\tau_c = 10^6$ ,  $10^9$ , and  $10^{12}$  yr), with labels showing the age values. Solid black lines represent magnetic field strength contours ( $B = 10^9$ ,  $10^{12}$ ,  $10^{14}$  G), and the solid black curve denotes the death line ( $P \propto P^{-2}$ ), beyond which coherent radio emission ceases. The diagram highlights the distinct evolutionary tracks of MSPs with lower  $P'$  values due to their rapid rotation and weaker magnetic fields.

The characteristic age of a pulsar,  $\tau_c$ , provides an estimate of its age based on its spin-down history. It is defined as:

$$\tau_c = \frac{P}{2\dot{P}},$$

where  $\tau_c$  is in years if  $P$  is in seconds and  $\dot{P}$  is in s/s (Lorimer, 2008). This age assumes that the pulsar has been spinning down at a constant rate since its birth, with an initial spin period much shorter than its current period. While this is a simplification, as the spin-down rate can vary due to magnetic field decay or environmental interactions, the characteristic age provides a useful first-order estimate. For example, the Crab Pulsar has a characteristic age of approximately 1,240 years, consistent with its known age from historical supernova records, whereas older pulsars like PSR J2145-0750 have characteristic ages on the order of  $10^9$  years (Manchester et al., 2005).

The spin-down process itself is governed by the energy loss due to magnetic dipole radiation, which can be expressed through the relation:

$$\dot{P} = \frac{8\pi^2 R^6 B^2 \sin^2 \alpha}{3c^3 I} P^{-1},$$

where  $R$  is the neutron star's radius (typically 10 km),  $I$  is the moment of inertia (approximately  $10^{45} \text{ g} \cdot \text{cm}^2$ ),  $\alpha$  is the angle between the rotation and magnetic axes, and  $c$  is the speed of light (Lorimer, 2008). This relation highlights the dependence of the spin-down rate on the magnetic field strength ( $B$ ) and the spin period ( $P$ ), illustrating why pulsars with stronger magnetic fields and shorter periods experience more rapid energy loss. For MSPs, the weaker magnetic field results in a significantly lower  $P$ , leading to slower spin-down rates and longer lifetimes (Igoshev et al., 2021).

These fundamental parameters and relations are often visualized in the  $P - P$  diagram, a powerful tool for understanding pulsar populations and their evolutionary pathways, as shown in Figure 1.

### 3. Evolutionary Mechanisms of Pulsars and MSPs

The evolution of pulsars and millisecond pulsars (MSPs) is governed by intricate physical processes that dictate their rotational dynamics and long-term behavior. At the core of these processes are two fundamental mechanisms: spin-up and spin-down, which drive the transformation of a neutron star—a compact remnant formed after a massive star's supernova explosion—into either a normal pulsar, with spin periods typically in the range of 0.1–10 seconds, or a millisecond pulsar (MSP), characterized by spin periods of 1–10 milliseconds. Spin-up refers to the acceleration of a neutron star's rotation, often through mechanisms like angular momentum transfer from a companion star in a binary system—a system where two stars orbit a common center of mass—or during the star's formation (Bhattacharya & van den Heuvel, 1991). This process is crucial for forming MSPs, reducing their spin period ( $P$ ) to the millisecond range. Conversely, spin-down describes the gradual deceleration of rotation due to energy loss mechanisms, such as magnetic dipole radiation—energy emitted as electromagnetic waves due to the rotating magnetic field—and particle wind—a stream of charged particles accelerated by the pulsar's magnetic field (Lorimer, 2008). These mechanisms determine key observables like the spin period ( $P$ ), spin period derivative ( $\dot{P}$ )—the rate of change of the spin period, and surface magnetic field ( $B$ ), which are influenced by intrinsic properties (e.g., moment of inertia ( $I$ )) and external factors (e.g., high stellar density in globular clusters (GCs)—dense stellar systems with  $10^4$ – $10^6$  stars—versus the Galactic field (GF)—the less dense regions of the Milky Way) (Han et al., 2021).

#### 3.1. Spin-Up: Types and Mechanisms

Spin-up occurs when a neutron star gains angular momentum, accelerating its rotation and transforming it into a rapidly rotating pulsar. This process can occur through various astrophysical scenarios, each involving distinct mechanisms and environments. Below, we explore four primary mechanisms that drive spin-up, as illustrated in Figure 2, highlighting the initial and final masses, as well as the internal phases of each mechanism.

##### 3.1.1. Accretion-Induced Spin-Up in Binaries

The most common pathway for spin-up is the recycling process in binary systems, particularly in low-mass X-ray binaries (LMXBs)—systems where a neutron star accretes material from a low-mass companion ( $< 1 M_{\odot}$ ). The process begins with a neutron star of mass  $\sim 1.4 M_{\odot}$  paired with a companion of  $0.1$ – $1 M_{\odot}$ . The companion evolves and expands, leading to a common envelope phase (CEP), where the neutron star spirals into the companion's envelope, losing orbital energy and shrinking the orbit to  $1$ – $10 R_{\odot}$ . This phase, marked in red in Figure 2, facilitates subsequent mass transfer (Ivanova et al., 2013). The companion then fills its Roche lobe—the gravitational equipotential surface beyond which material is no longer bound to the star—initiating Roche lobe overflow (RLOF), where material is transferred to the neutron star, forming an accretion disk. The accretion-induced torque transfers angular momentum, spinning up the neutron star to a millisecond pulsar (MSP) with a spin period of  $P \sim 1$ – $10 \text{ ms}$ . The final system consists of an MSP ( $\sim 1.4 M_{\odot}$ ) and a white dwarf companion, a degenerate stellar remnant (Bhattacharya & van den Heuvel, 1991). Observational evidence includes MSPs like SAX J1808.4-3658, detected by the Rossi X-ray Timing Explorer (RXTE), with a spin period of 2.5 ms (Wijnands et al., 2005).

The efficiency of this torque depends on the mass accretion rate ( $\dot{M}$ )—typically  $10^{-10}$ – $10^{-8} M_{\odot}/\text{yr}$ —and the Alfvén radius, where the magnetic field balances the accretion flow. During accretion, the magnetic field is suppressed through diamagnetic screening, where accreted material buries the field, reducing it from  $10^{12}$  Gauss to  $10^{8}$ – $9$  Gauss, a process critical for MSP formation (Han et al., 2021). If the accretion rate exceeds

## Spin-Up

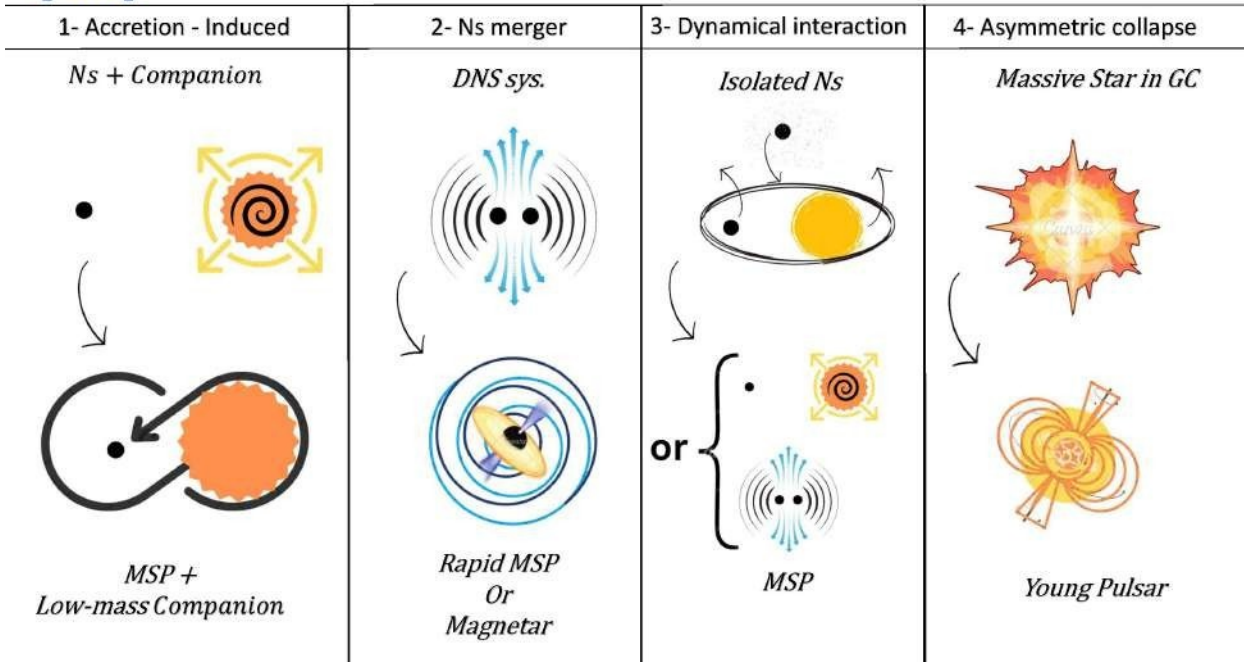


Figure 2. Schematic illustration of the four primary spin-up mechanisms for neutron stars: Accretion-Induced Spin-Up in Binaries, Spin-Up via Neutron Star Mergers, Spin-Up via Dynamical Interactions in Clusters, and Spin-Up from Asymmetric Collapse. Each column shows the initial and final states. The columns are aligned to allow comparison of evolutionary stages across mechanisms.

the Eddington limit—the maximum luminosity at which radiation pressure balances gravitational attraction—super-Eddington accretion can trigger disk instabilities, potentially halting the spin-up (Chatopadhyay et al., 2021). This mechanism is prevalent in both the Galactic field and globular clusters, where binary systems are common (Chen et al., 2021).

### 3.1.2. Spin-Up via Neutron Star Mergers

Spin-up can also occur during NS-NS mergers in double neutron star systems (DNS), starting with two neutron stars ( $\sim 1.4 M_{\odot}$  each). The process involves orbital decay due to gravitational wave emission, shrinking the orbit over  $10^8$  –  $10^9$  years. The merger phase, marked in red in Figure 2, transfers orbital angular momentum to the remnant, increasing its spin frequency to over 700 Hz, potentially forming a rapidly rotating MSP or a magnetar—a neutron star with an extremely strong magnetic field ( $B \sim 10^{14}$  –  $10^{15}$  Gauss). This is followed by magnetic field amplification via dynamo processes—mechanisms that generate magnetic fields through rotational motion in a conductive fluid—resulting in a final mass of  $1.4$  –  $2.5 M_{\odot}$  or a black hole if the mass exceeds the Tolman-Oppenheimer-Volkoff limit ( $\sim 2.5 M_{\odot}$ ) (Rezzolla et al., 2018). Observational signatures include short gamma-ray bursts (GRBs) and kilonovae, such as GW170817, detected by LIGO and Virgo (Abbott et al., 2017).

The merger remnant may form a debris disk, which can lead to wind accretion—accretion of material from a disk-driven wind—further enhancing the spin-up. This mechanism is significant in dense environments like globular clusters, where the merger rate is higher due to dynamical interactions (Hui et al., 2010). The amplified magnetic field can lead to rapid energy loss, potentially transitioning the remnant into a spin-down phase, as discussed in the next section (Giacomazzo et al., 2015).

### 3.1.3. Spin-Up via Dynamical Interactions in Clusters

In globular clusters (GCs), dynamical interactions driven by high number density ( $\sim 10^5$  stars/pc $^3$ ) facilitate spin-up. A neutron star ( $\sim 1.4 M_{\odot}$ ) undergoes dynamical capture, where it gravitationally captures a companion star through close encounters, followed by binary formation with a main-sequence star, as shown in red in Figure 2. This leads to RLOF + accretion, where the companion transfers material, spinning up the neutron star to an MSP ( $\sim 1.4 M_{\odot}$ ) with a spin period of 1 – 10 ms. The high

interaction rate in Gcs enhances MSP formation, as evidenced by population studies in the ATNF Pulsar Catalog, which lists over 150 MSPs in GCs (Manchester et al., 2005).

The tidal circularization process—where tidal forces circularize the binary orbit over  $10^5$  –  $10^6$  years—and tidal heating play a key role in stabilizing the binary, facilitating sustained mass transfer (Rasio & Shapiro, 1994). This mechanism often leads to exotic systems like black widow pulsars, where the neutron star's radiation ablates the companion, as seen in PSR J1959+2048 (Hui et al., 2010).

### 3.1.4. Spin-Up from Asymmetric Collapse

During the formation of a neutron star via a core-collapse supernova, a massive progenitor star ( $> 8 M_{\odot}$ ) undergoes core collapse, where the core implodes under gravity. If the collapse is asymmetric—due to turbulent convection or rotational instabilities—the resulting neutron star ( $\sim 1.4 M_{\odot}$ ) inherits a rapid initial spin period ( $P_0$ ) of 10–100 ms, as shown in red in Figure 2. This phase is followed by the formation of a neutron star, marked by the onset of natal kicks—impulses that can impart velocities of 100 – 500 km/s to the neutron star—leading to a young pulsar (Burrows et al., 2007). The initial magnetic field ( $B_0$ ) can be amplified via dynamo processes in the superfluid core—a state where neutrons form a frictionless fluid—resulting in a surface magnetic field of  $10^{12}$  –  $10^{14}$  Gauss, as seen in pulsars like PSR J0537-6910, observed by the Chandra X-ray Observatory (Kargaltsev & Pavlov, 2008).

The rapid rotation often triggers early spin-down mechanisms, such as magnetic braking or gravitational wave emission, particularly if the neutron star forms a supernova remnant (SNR)—a shell of ejected material—or a pulsar wind nebula (PWN)—a nebula powered by the pulsar's relativistic wind. This mechanism is critical for understanding the initial conditions of young pulsars and their subsequent evolution (Duncan & Thompson, 1996).

## 3.2. Spin-Down: Types and Mechanisms

Spin-down occurs when a pulsar loses rotational energy, reducing its spin frequency over time. This process is driven by various energy loss mechanisms, which dominate after the spin-up phase and shape the pulsar evolutionary track on the P-P' diagram—a plot of spin period versus its derivative used to study pulsar evolution. The  $P$  –  $E$  diagram, shown in Figure 4, complements this by illustrating the rotational energy loss ( $E$ ) across different pulsar populations, providing a deeper understanding of spin-down dynamics. Below, we discuss five key spin-down mechanisms, as illustrated in Figure 3, detailing their initial and final states and internal phases.

### 3.2.1. Magnetic Dipole Radiation Spin-Down

The dominant spin-down mechanism for most pulsars is magnetic dipole radiation, starting with a young pulsar ( $\sim 1.4 M_{\odot}$ ) with a spin period of 10 – 100 ms. The rotating magnetosphere—the region where the magnetic field dominates the plasma dynamics—emits electromagnetic waves, carrying away energy, as shown in blue in Figure 3. This magnetic dipole braking phase increases the spin period to 1 – 10 s, resulting in an older pulsar. The energy loss rate scales with the surface magnetic field ( $B$ ) and spin frequency, following  $P \propto B^2 P^{-1}$ , as seen in the Crab Pulsar (PSR B0531+21) with  $P \approx 4.2 \times 10^{-13}$  s/s (Barr et al., 2017).

The process is most effective in isolated pulsars with strong magnetic fields ( $B \sim 10^{12}$  Gauss), where the spin-down luminosity—the rate of rotational energy loss—powers phenomena like pulsar wind nebulae (PWNe), aligning with the lower  $E$  values ( $10^{31}$  –  $10^{33}$  erg/s) observed for normal pulsars in Figure 4. Over time, the pulsar's characteristic age ( $\tau_c = P/(2P')$ ) increases, often reaching  $10^6$  –  $10^9$  years, as observed in pulsars cataloged by the ATNF Pulsar Catalog (Manchester et al., 2005). This mechanism is fundamental to understanding the long-term evolution of normal pulsars (Lorimer, 2008).

### 3.2.2. Magnetic Field Decay Spin-Down

Over long timescales, magnetic field decay reduces the efficiency of magnetic dipole radiation for an active pulsar ( $\sim 1.4 M_{\odot}$ ). The Ohmic dissipation phase, where electrical resistance in the crust dissipates the magnetic field, leads to field decay, as shown in blue in Figure 3, pushing the pulsar toward the pulsar death line—the threshold on the P-P' diagram where coherent radio emission ceases. For MSPs, this decay significantly slows the spin-down rate, with  $P \sim 10^{-20}$  s/s, as seen in population synthesis studies (Gonthier et al., 2018).

## Spin-Down

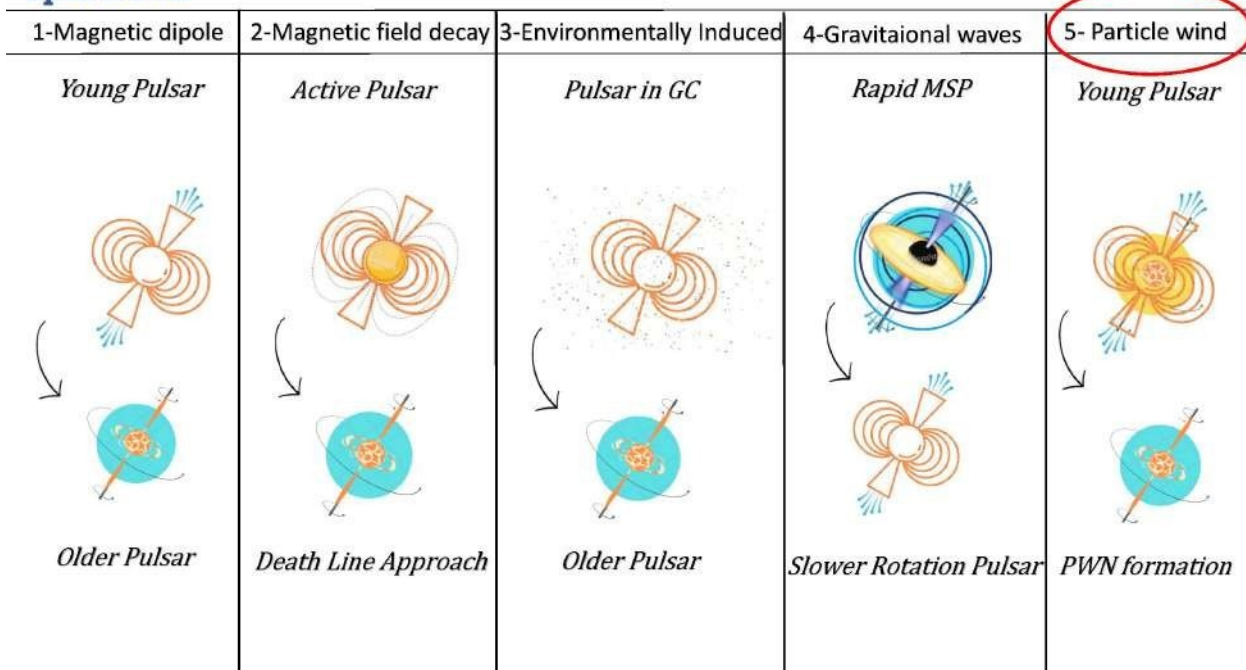


Figure 3. Schematic illustration of the five primary spin-down mechanisms for pulsars: Magnetic Dipole Radiation Spin-Down, Magnetic Field Decay Spin-Down, Environmentally Induced Spin-Down, Gravitational Wave Spin-Down, and Particle Wind Spin-Down. Each column shows the initial and final states. The columns are aligned to allow comparison of evolutionary stages across mechanisms. Particle Wind Spin-Down will ignore for following scenarios

The Hall effect—a process where the magnetic field evolves due to the motion of charged particles in the crust—further contributes to field decay over  $10^7$  –  $10^9$  years, as observed in older pulsars like PSR J2145-0750 (Igoshev et al., 2021). This mechanism aligns with the gradual decline in  $E$  for older pulsars near the death line in Figure 4, making it critical for understanding the late stages of pulsar evolution, particularly in the Galactic field, where external interactions are minimal (Manchester et al., 2005).

### 3.2.3. Environmentally Induced Spin-Down

In globular clusters (GCs), a GC pulsar ( $\sim 1.4 M_{\odot}$ ) experiences dynamical interactions due to the high stellar density, leading to orbital decay in binary systems, as shown in blue in Figure 3. This results in accelerated spin-down, where the pulsar rotation slows more rapidly due to tidal locking—a state where the rotational and orbital periods synchronize. This mechanism is contrasted with isolated pulsars in the Galactic field (GF), which experience slower spin-down (Freire, 2022).

The tidal circularization process in binaries enhances energy loss, with timescales of  $10^5$  –  $10^6$  years, as seen in pulsars like PSR J1959+2048 in GCs (Manchester et al., 2005). This mechanism highlights the role of environment in shaping pulsar evolution, particularly in dense stellar systems where dynamical interactions are frequent, influencing the  $E$  distribution observed in Figure 4 for GC pulsars (Verbunt & Freire, 2014).

### 3.2.4. Gravitational Wave Spin-Down

Spin-down can occur through gravitational waves if a rapid MSP ( $\sim 1.4 M_{\odot}$ ) exhibits mass asymmetry, such as ellipticity ( $\epsilon$ )—a measure of the star’s deformation from a perfect sphere—as shown in blue in Figure 3. The mass asymmetry development phase leads to gravitational wave emission, where energy is radiated as spacetime ripples, slowing the rotation to a slower rotation state. This mechanism is significant for rapidly rotating MSPs, as explored in LIGO searches for continuous gravitational waves from pulsars like PSR J0437-4715, which has a spin frequency of  $\sim 174$  Hz (Abbott et al., 2020).

The energy loss rate depends on the moment of inertia ( $I$ ) and the ellipticity, providing insights into the superfluid core and crustal magnetic field—the magnetic field anchored in the neutron star’s solid crust. This mechanism aligns with the higher  $E$  values ( $10^{34}$  –  $10^{36}$  erg/s) observed for MSPs in Figure 4, particularly

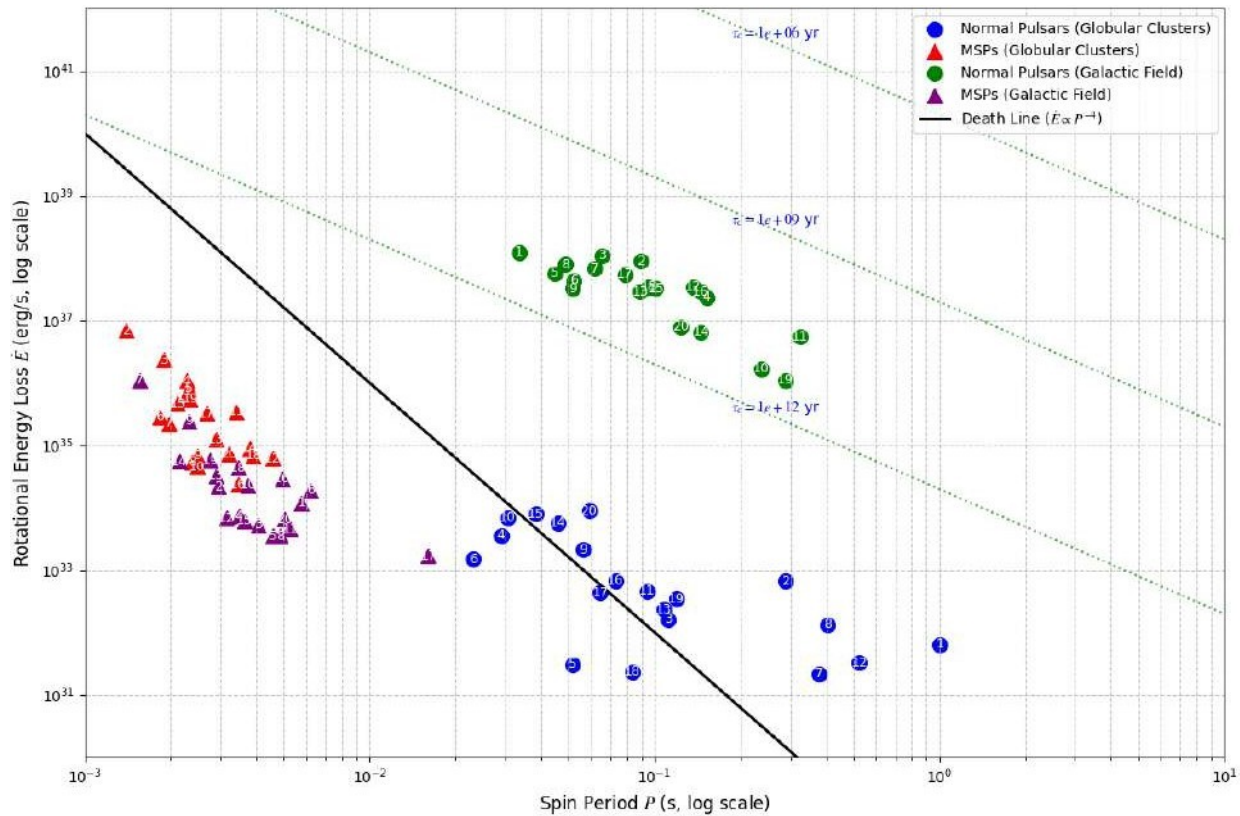


Figure 4.  $P - E$  diagram illustrating the distribution of four pulsar sub-populations: normal pulsars in globular clusters (blue circles), millisecond pulsars (MSPs) in globular clusters (red triangles), normal pulsars in the Galactic field (green circles), and MSPs in the Galactic field (purple triangles), numbered according to Tables 1, 2, 3, and 4. The x-axis spans spin periods from  $10^{-3}$  to  $10^1$  s, and the y-axis covers rotational energy loss from  $10^{30}$  to  $10^{42}$  erg/s, both on logarithmic scales. Dotted green lines indicate characteristic age contours ( $\tau_c = 10^6$ ,  $10^9$ , and  $10^{12}$  yr), with labels showing the age values. The solid black curve represents the death line ( $E \propto P^{-4}$ ), beyond which coherent radio emission ceases. The diagram reveals that MSPs exhibit Higher  $E$  values due to their rapid rotation, while normal pulsars cluster at lower  $E$  values, reflecting slower spin-down driven by magnetic dipole radiation and particle winds.

in binary systems where orbital dynamics enhance asymmetry (Riles, 2017). Theoretical models suggest that gravitational wave emission could dominate spin-down in the first  $10^5$  years of an MSP life (Kamlah et al., 2022).

### 3.2.5. Particle Wind Spin-Down

Pulsars also lose energy through particle winds, starting with a young pulsar ( $\sim 1.4 M_\odot$ ). The particle acceleration phase, shown in blue in Figure 3, involves charged particles being accelerated in the magnetosphere, leading to particle wind emission—a stream of relativistic particles that carries away rotational energy. This results in the formation of a pulsar wind nebula (PWN), a glowing nebula powered by the wind, as observed in the Vela Pulsar (PSR B0833-45) by the Fermi Gamma-ray Space Telescope (Abdo et al., 2009).

The interplay between particle wind and magnetic dipole radiation shapes the pulsar emission properties, with the wind contributing significantly to the spin-down luminosity in younger pulsars ( $\tau_c \sim 10^4 - 10^5$  years). The energy loss rate depends on the magnetic field strength and spin frequency, often leading to a PWN in the interstellar medium (ISM)—the material between stars, aligning with the energy loss trends observed in Figure 4 for normal pulsars (Shi & Ng, 2024). This mechanism provides insights into the high-energy emission processes of pulsars (Kalapotharakos et al., 2014).

## 4. Evolutionary Scenarios

The evolutionary pathways of neutron stars into pulsars and millisecond pulsars (MSPs) are shaped by a combination of spin-up and spin-down mechanisms, influenced by environmental factors and binary interactions. These pathways lead to diverse outcomes, from isolated pulsars to rapidly spinning MSPs, and even the formation of black holes through mergers. Below, we outline seven distinct scenarios, supported by observational evidence and theoretical models, as illustrated in Figure 5, detailing their initial and final masses and internal phases.

### 4.1. Isolated Pulsar Formation and Evolution

A massive star ( $> 8 M_{\odot}$ ) undergoes a core-collapse supernova, forming a neutron star with a mass of  $\sim 1.4 M_{\odot}$ . The core collapse phase, marked in red in Figure 5, involves an asymmetric collapse (Spin-Up: Asymmetric Collapse), where turbulent convection imparts a rapid initial spin period ( $P_0 \sim 10 - 100$  ms) and a natal kick with a velocity of  $100 - 500$  km/s. This is followed by magnetic dipole braking (Spin-Down: Magnetic Dipole Radiation), shown in blue, where the rotating magnetosphere emits electromagnetic waves, increasing the spin period to  $1 - 10$  s over  $10^6 - 10^9$  years. The final phase, field decay (Spin-Down: Magnetic Field Decay), reduces the surface magnetic field ( $B$ ) from  $10^{12}$  Gauss to  $10^{10}$  Gauss via Ohmic dissipation, pushing the pulsar toward the pulsar death line (Burrows et al., 2007, Igoshev et al., 2021).

The resulting isolated pulsar powers a pulsar wind nebula (PWN) via its spin-down luminosity ( $L_{sd} \propto B^2 P^{-4}$ ), as seen in pulsars like PSR J0537-6910, observed by the Chandra X-ray Observatory (Kargaltsev & Pavlov, 2008). If the pulsar moves supersonically through the interstellar medium (ISM), it may create a bow shock, as observed in the Guitar Nebula (Gaensler & Slane, 2006). This scenario is typical for normal pulsars in the Galactic field, where dynamical interactions are minimal, aligning with the lower  $E$  values observed in Figure 4 (Lorimer, 2008).

### 4.2. Isolated MSP After Companion Disruption

Following the recycling process in a binary system, an MSP ( $\sim 1.4 M_{\odot}$ ) with a low-mass companion undergoes companion disruption (Spin-Up: Accretion-Induced Spin-Up, reflecting prior accretion), shown in red in Figure 5, where the companion is ablated by the pulsar radiation, forming a black widow pulsar. The slow spin-down phase (Spin-Down: Magnetic Dipole Radiation), shown in blue, follows, with a spin period derivative ( $P \sim 10^{-20} - 10^{-19}$  s/s), leading to a stable MSP state. The final outcome is an isolated MSP ( $\sim 1.4 M_{\odot}$ ) (Zhu et al., 2024).

A debris disk may form from the companion remnants, potentially detectable in infrared wavelengths, as seen in systems like PSR J1959+2048 (Hui et al., 2010). The slow spin-down ensures the MSP remains active for billions of years, as observed in pulsars like PSR J0437-4715 in the ATNF Pulsar Catalog (Manchester et al., 2005). This scenario is common in globular clusters, with energy loss patterns aligning with the higher

$E$  values for MSPs in Figure 4 (Freire, 2022).

### 4.3. MSP Formation via Accretion in a Binary System

A neutron star ( $\sim 1.4 M_{\odot}$ ) in a low-mass X-ray binary (LMXB) with a companion ( $0.1 - 1 M_{\odot}$ ) undergoes common envelope evolution (CEE) (Spin-Up: Accretion-Induced Spin-Up), shown in red in Figure 5, where the neutron star spirals into the companion envelope, ejecting it and forming a post-common envelope binary (PCEB) with a close orbit ( $1 - 10 R_{\odot}$ ). The RLOF + accretion phase (Spin-Up: Accretion-Induced Spin-Up) follows, where the companion transfers material via Roche lobe overflow, spinning up the neutron star to an MSP with a spin period of  $1 - 10$  ms. The final phase, field suppression (Spin-Down: Magnetic Field Decay), shown in blue, reduces the surface magnetic field to  $10^{8-9}$  Gauss, resulting in an MSP ( $\sim 1.4 M_{\odot}$ ) and a white dwarf companion (Bhattacharya & van den Heuvel, 1991).

The mass accretion rate ( $\dot{M} \sim 10^{-10} - 10^{-8} M_{\odot}/\text{yr}$ ) and viscous dissipation in the accretion disk sustain the spin-up, while tidal locking circularizes the orbit over  $10^6$  years (Rasio & Shapiro, 1994). Observational evidence includes X-ray pulsations from MSPs like SAX J1808.4-3658, detected by the Rossi X-ray Timing Explorer (RXTE) (Wijnands et al., 2005). This scenario is prevalent in both the Galactic field and globular clusters, with higher  $E$  values for MSPs as seen in Figure 4 (Chen et al., 2021).

#### 4.4. MSP Formation via Dynamical Interactions in Globular Clusters

In globular clusters (GCs), a neutron star ( $\sim 1.4 M_{\odot}$ ) experiences dynamical capture (Spin-Up: Dynamical Interactions in Clusters), shown in red in Figure 5, forming a binary with a main-sequence star through tidal capture. The RLOF + accretion phase (Spin-Up: Accretion-Induced Spin-Up) follows, spinning up the neutron star to an MSP with a spin period of  $1 - 10$  ms. The tidal circularization phase (Spin-Down: Environmentally Induced Spin-Down), shown in blue, stabilizes the orbit, resulting in an MSP ( $\sim 1.4 M_{\odot}$ ) (Verbunt & Freire, 2014).

The tidal circularization timescale ( $\sim 10^5 - 10^6$  years) and tidal heating facilitate sustained mass transfer, as seen in MSPs in 47 Tucanae, where 25 MSPs with  $P < 10$  ms have been identified using the Parkes Telescope (Freire, 2022). The high binary fraction in GCs ( $\sim 50\%$ ) underscores the role of dynamical interactions in MSP formation, with energy loss patterns reflected in Figure 4 (Freire, 2022). This scenario highlights the environmental influence on pulsar evolution in dense stellar systems (Hui et al., 2010).

#### 4.5. Pulsar in a Wide Binary Without Roche Lobe Overflow

A neutron star ( $\sim 1.4 M_{\odot}$ ) forms in a binary system with a wide orbit ( $a \sim 10 - 100$  AU) and a companion star (main-sequence or evolved), which does not undergo Roche lobe overflow. The neutron star evolves as an isolated pulsar, experiencing magnetic dipole radiation (Spin-Down: Magnetic Dipole Radiation), shown in blue in Figure 5, where energy loss increases the spin period ( $P$ ) over  $10^9$  years. This is followed by orbital decay (Spin-Down: Gravitational Wave Spin-Down), where gravitational waves shrink the orbit, potentially leading to a merger if the companion evolves into a neutron star. The final system remains a binary with a pulsar ( $\sim 1.4 M_{\odot}$ ) and its companion (Chen et al., 2021).

This scenario results in a slow spin-down rate ( $P \sim 10^{-20}$  s/s), as seen in pulsars like PSR J2145-0750, which has a weak crustal magnetic field ( $B \sim 10^9$  Gauss) (Manchester et al., 2005). The low binary fraction ( $\sim 5\%$ ) in the Galactic field (GF) underscores the rarity of dynamical interactions in this environment, making this scenario a common evolutionary path for pulsars in wide binaries, with energy loss patterns consistent with Figure 4 (Manchester et al., 2005).

#### 4.6. NS-NS Merger Leading to MSP or Black Hole

In a double neutron star system (DNS), two neutron stars ( $\sim 1.4 M_{\odot}$  each) undergo orbital decay (Spin-Down: Gravitational Wave Spin-Down), shown in blue in Figure 5, over  $10^8 - 10^9$  years, leading to an NS-NS merger (Spin-Up: Neutron Star Mergers), shown in red. The merger transfers orbital angular momentum, producing a rapidly spinning MSP with a spin frequency exceeding 700 Hz. The field amplification phase (Spin-Down: Magnetic Dipole Radiation), shown in blue, follows, where dynamo processes amplify the core magnetic field to  $10^{13}$  Gauss. The final outcome is an MSP ( $\sim 1.4 - 2.5 M_{\odot}$ ) or a black hole if the mass exceeds  $2.5 M_{\odot}$  (Rezzolla et al., 2018).

A debris disk forms, contributing to short gamma-ray bursts (GRBs) and kilonovae, as observed in GW170817 by LIGO and Virgo (Abbott et al., 2017). This scenario is more likely in globular clusters, where the merger rate is enhanced by dynamical interactions, with higher  $E$  values for the resulting MSPs as seen in Figure 4 (Hui et al., 2010). The amplified magnetic field can lead to rapid energy loss, shaping the remnant long-term evolution (Giacomazzo et al., 2015).

#### 4.7. NS-BH Merger and Removal

A neutron star ( $\sim 1.4 M_{\odot}$ ) in a binary with a stellar-mass black hole ( $5 - 20 M_{\odot}$ ) undergoes orbital decay (Spin-Down: Gravitational Wave Spin-Down), shown in blue in Figure 5, over  $10^9$  years. The tidal disruption phase (Spin-Down: Gravitational Wave Spin-Down) follows, where the neutron star is disrupted by the black hole tidal forces, leading to a merger. The final outcome is a black hole ( $> 5 M_{\odot}$ ), removing the neutron star from the pulsar population (Chen et al., 2021).

This process may produce a kilonova and short gamma-ray bursts, detectable by LIGO and Virgo, though no confirmed NS-BH mergers have been observed as of May 2025 (Abbott et al., 2020). This scenario, though rare, is significant in shaping pulsar population statistics, particularly in the Galactic field, where such binaries can form through stellar evolution, with energy loss dynamics consistent with Figure 4 (Perna et al., 2018). The merger highlights the role of gravitational waves in the final stages of compact binary evolution (Abbott et al., 2020).

## 5. Challenges in Modeling Pulsar Evolution

Modeling the evolution of pulsars and millisecond pulsars (MSPs) is a complex task that involves simulating a wide range of physical processes over timescales spanning millions to billions of years. Despite significant advancements in theoretical and computational techniques, several key challenges persist, hindering our ability to fully understand the evolutionary pathways of these objects. These challenges primarily revolve around the long-term evolution of magnetic fields, the dynamics of binary interactions, and the computational limitations of simulations in dense stellar environments (Liu et al., 2021).

One of the primary challenges in modeling pulsar evolution is accurately capturing the long-term evolution of their magnetic fields. Magnetic field decay, driven by processes such as Ohmic dissipation and the Hall effect, occurs over timescales of  $10^6$  to  $10^9$  years and significantly influences spin-down rates (Igoshev et al., 2021). Ohmic dissipation involves the conversion of magnetic energy into heat due to electrical resistance in the neutron stars crust, while the Hall effect introduces non-linear interactions between magnetic fields and electric currents, complicating the decay process. Current models struggle to incorporate these effects with sufficient precision, as they require detailed knowledge of the neutron stars internal composition, temperature evolution, and conductivity, which are poorly constrained by observations (Igoshev et al., 2021). For MSPs, which undergo magnetic field suppression during the recycling process, the challenge is even greater, as the interplay between accretion-induced field burial and subsequent decay remains poorly understood (Chattopadhyay et al., 2021). These uncertainties lead to discrepancies between theoretical predictions and observational data, such as the observed spin-down rates of older pulsars like PSR J2145-0750 (Manchester et al., 2005).

Another significant challenge lies in modeling the dynamics of binary interactions, which are crucial for the formation and evolution of MSPs through the recycling process. Binary interactions involve complex processes such as mass transfer, angular momentum exchange, and orbital evolution, all of which are influenced by factors like the companion stars mass, the binaries orbital period, and the neutron stars magnetic field (Chattopadhyay et al., 2021). Current models often rely on simplified assumptions, such as constant mass accretion rates or idealized Roche-lobe overflow, which fail to capture the stochastic nature of these interactions. For instance, the episodic nature of accretion in low-mass X-ray binaries (LMXBs) can lead to variations in the spin-up efficiency, affecting the final spin period of the MSP (Bhattacharya & van den Heuvel, 1991). Furthermore, the long-term orbital evolution of binary systems, including the effects of gravitational wave emission and tidal interactions, adds another layer of complexity that current models struggle to address comprehensively (Belczynski et al., 2016).

In dense stellar environments like globular clusters (GCs), these challenges are compounded by the need to simulate dynamical interactions on a large scale. N-body simulations, such as those performed using NBODY6++GPU, are essential for modeling the evolution of pulsars in GCs, where frequent stellar encounters drive binary formation and disruption (Wang et al., 2015). However, these simulations face significant computational limitations, particularly in resolving the dense cores of GCs, where stellar densities can exceed  $10^5$  stars per cubic parsec (e.g., Kamlah et al., 2022). The high computational cost of tracking individual stellar interactions over long timescales often forces researchers to use simplified prescriptions for binary evolution and neutron star dynamics, reducing the accuracy of the models. For example, accurately simulating the formation of MSPs through dynamical encounters requires resolving both the short-timescale interactions (e.g., close encounters) and the long-timescale evolution of the cluster, a task that remains computationally prohibitive. These limitations hinder our ability to predict the population statistics of MSPs in GCs, such as their spin period distributions and binary fractions, which are critical for comparison with observational data (Freire, 2022).

Addressing these challenges requires the development of more sophisticated theoretical models and computational techniques. For magnetic field evolution, incorporating detailed microphysical models of neutron star interiors, such as temperature-dependent conductivity and multi-fluid dynamics, could improve the accuracy of decay predictions (Igoshev et al., 2021). For binary interactions, hybrid approaches that combine detailed stellar evolution codes with N-body simulations may offer a path forward, allowing for more realistic modeling of mass transfer and orbital dynamics (Belczynski et al., 2016). Finally, advancements in computational power and algorithms, such as the use of machine learning to accelerate N-body simulations, could help overcome the current limitations in modeling dense stellar environments (such as, e.g., Wang et al., 2015). Until these challenges are addressed, our understanding of pulsar evolution will remain incomplete, underscoring the need for continued theoretical and observational efforts.

The NBODY6++GPU framework encounters challenges in fully capturing the complexity of pulsar evolution.

tion, particularly in addressing certain key interactions that influence stellar behavior. Limited computational resources reduce the accuracy of long-term magnetic field modeling, while the absence of support for some energy loss mechanisms narrows the range of possible predictions. Additionally, lower resolution in dense stellar environments hinders accurate population synthesis, creating gaps in our understanding. These areas highlight the need for targeted enhancements to strengthen the capabilities of NBODY6++GPU ([Spurzem & Kamlah, 2023](#)).

## 6. Discussion and Future Directions

This study has provided a comprehensive examination of the evolutionary mechanisms governing pulsars and millisecond pulsars (MSPs), building on the statistical insights from the first paper in this series ([Rah et al., 2024](#)). We have explored the fundamental processes of spin-up and spin-down, emphasizing the roles of accretion, magnetic field decay, and binary interactions in shaping the rotational and magnetic properties of these compact objects. Our analysis of environmental influences has highlighted stark contrasts between globular clusters (GCs) and the Galactic field (GF), with GCs fostering a higher prevalence of MSPs due to frequent dynamical interactions, while the GF is dominated by isolated pulsars undergoing slower evolutionary changes ([Freire, 2022](#), [Zhang et al., 2023](#)). Additionally, we have identified key challenges in modeling pulsar evolution, including the complexities of long-term magnetic field decay, the dynamics of binary interactions, and the computational limitations of N-body simulations in dense stellar environments ([Igoshev et al., 2021](#)). Recent observational advancements have significantly enriched our understanding of pulsar evolution.

Observations from instruments like FAST and CHIME have revealed the diverse evolutionary pathways of pulsars, particularly through the identification of transitional millisecond pulsars (tMSPs) and black widow pulsars. tMSPs, which alternate between accretion-powered and rotation-powered states, offer a unique window into the recycling process, while black widow pulsars in GCs highlight the impact of dynamical interactions on the formation of exotic systems ([Bahramian et al., 2018](#), [Hui et al., 2010](#)). These findings underscore the importance of integrating new observational data into theoretical models, particularly to account for the stochastic nature of binary interactions and the long-term effects of magnetic field decay ([Chattopadhyay et al., 2021](#)).

Looking ahead, several critical areas warrant further investigation to advance our understanding of pulsar evolution. One pressing need is the development of more sophisticated models for magnetic field evolution, which remains poorly constrained due to the intricate interplay of Ohmic dissipation, the Hall effect, and accretion-induced field burial ([Igoshev et al., 2021](#)). Future research should focus on incorporating detailed microphysical models of neutron star interiors, such as temperature-dependent conductivity and multi-fluid dynamics, to improve the accuracy of field decay predictions and their impact on spin-down rates. Another priority is the refinement of models for binary interactions, particularly for systems undergoing the recycling process. Hybrid approaches that combine detailed stellar evolution codes with N-body simulations could provide a more realistic framework for modeling mass transfer, orbital evolution, and the episodic nature of accretion ([Belczynski et al., 2016](#)).

The unique environment of globular clusters, characterized by high stellar densities and frequent dynamical interactions, presents a rich area for future exploration. Ongoing research efforts are leveraging updated NBODY6++GPU simulations to study the evolution of pulsars and MSPs in GCs, aiming to address the computational challenges identified in this study ([Spurzem & Kamlah, 2023](#)). These investigations will focus on improving prescriptions for binary evolution and neutron star dynamics, providing a clearer picture of MSP formation, spin period distributions, and binary fractions in GCs, which can be directly compared with observational data from clusters like 47 Tucanae and M28 ([Freire, 2012](#), [Zhang et al., 2023](#)).

Furthermore, the diverse population of pulsars, including exotic systems such as black widow pulsars and tMSPs, requires continued attention to fully elucidate their evolutionary pathways. Future studies are in progress to develop detailed models of magnetic field evolution in these systems, with a particular emphasis on the role of accretion and ablation in shaping their properties. These efforts will also leverage recent multi-wavelength observations, such as those from FAST and Fermi, to constrain theoretical models of pulsar emission and magnetic field decay ([Abdo et al., 2009](#), [Bahramian et al., 2018](#)). By addressing these topics, the future research aims to bridge the gap between observational data and theoretical predictions, offering a more comprehensive understanding of the evolution of pulsars across different environments and

evolutionary stages.

Building on earlier theoretical work, the next phase will focus on integrating advanced computational methods to conduct detailed pulsar simulations using NBODY6++GPU. In Article III, which is in progress and under review for publication in this series (Rah et al., 2024), we will develop custom algorithms and incorporate improved models into NBODY6++GPU to accurately reflect stellar evolution across different settings. This process will involve repeated testing and validation of the simulation results to ensure reliable predictions about pulsar populations and their observable traits. Future efforts will connect theoretical insights with practical simulations, advancing our understanding of cosmic dynamics (Spurzem & Kamlah, 2023).

## 7. Conclusion

The evolution of neutron stars into pulsars and MSPs is governed by intricate spin-up and spin-down mechanisms, as well as diverse evolutionary scenarios. From asymmetric collapse to recycling in binary systems, dynamical interactions in globular clusters, and NS-NS mergers, these pathways shape the evolutionary tracks of pulsars on the P- $P'$  diagram. Future population synthesis studies and observations with LIGO and Virgo will further elucidate these processes (Shi & Ng, 2024, Zhang et al., 2023). The integration of advanced simulations, refined physical models, and multi-wavelength observations will be crucial for addressing the remaining challenges and uncovering the full complexity of pulsar evolution. Future investigations, as outlined, will build on the foundation laid here, providing deeper insights into the intricate processes that govern these fascinating compact objects.

This study showcases the strength of NBODY6 ++ GPU in utilizing robust theoretical frameworks and formulas derived from scenario analyzes to confidently model the evolution of pulsars (Spurzem & Kamlah, 2023). These reliable mathematical foundations, shaped by thorough scenario studies, enable accurate predictions of stellar behavior and energy loss patterns. This success supports future research on exploring complex pulsar systems, providing a solid foundation for population studies and analyses across various environments. The integration of these principles ensures a promising future for deepening our understanding of the most mysterious objects in the universe.

## Acknowledgments

This work was supported by the Byurakan Astrophysical Observatory (BAO). MR gratefully acknowledges the academic and financial support received from BAO throughout her Ph.D. studies.

FFD and RS acknowledge support by the German Science Foundation (DFG), priority program SPP 1992 "Exploring the diversity of extrasolar planets" (project Sp 345/22-1 and central visitor program), and by DFG project Sp 345/24-1.

RS acknowledges NAOC International Cooperation Office for its support in 2023, 2024, and 2025, and support by the National Natural Science Foundation of China (NSFC) under grant No. 12473017.

## References

Abbott B. P., et al., 2017, *Physical review letters*, 119, 161101

Abbott B. P., et al., 2020, *The Astrophysical Journal*, 892, L3

Abdo A. A., et al., 2009, *The Astrophysical Journal*, 696, 1084

Bahramian A., et al., 2018, , 864, 28

Barr E., Freire P., Kramer M., Champion D., Berezina M., Bassa C., Lyne A., Stappers B., 2017, *Monthly Notices of the Royal Astronomical Society*, 465, 1711

Belczynski K., et al., 2016, , 594, A97

Bhattacharya D., van den Heuvel E. P. J., 1991, *Physics Reports*, 203, 1

Burrows A., Dessart L., Livne E., Ott C. D., Murphy J., 2007, *The Astrophysical Journal*, 664, 416

Chattopadhyay D., Stevenson S., Hurley J. R., Bailes M., Broekgaarden F., 2021, , [504, 3682](#)

Chen H.-L., Tauris T. M., Han Z., Chen X., 2021, Monthly Notices of the Royal Astronomical Society, 503, 3540

Demorest P. B., Pennucci T., Ransom S. M., Roberts M. S. E., Hessels J. W. T., 2010, , [467, 1081](#)

Duncan R. C., Thompson C., 1996, in AIP Conference Proceedings. pp 111–117

Freire P. C., 2012, Proceedings of the International Astronomical Union, 8, 243

Freire P. C., 2022, arXiv preprint arXiv:2204.13468

Gaensler B. M., Slane P. O., 2006, Annu. Rev. Astron. Astrophys., 44, 17

Galloway D. K., Keek L., 2021, in Belloni T. M., M\'endez M., Zhang C., eds, Astrophysics and Space Science Library Vol. 461, Timing Neutron Stars: Pulsations, Oscillations and Explosions. pp 209–262 ([arXiv:1712.06227](#)), [doi:10.1007/978-3-662-62110-3\\_5](#)

Giacomazzo B., Zrake J., Duffell P. C., MacFadyen A. I., Perna R., 2015, The Astrophysical Journal, 809, 39

Gonthier P. L., Harding A. K., Ferrara E. C., Frederick S. E., Mohr V. E., Koh Y.-M., 2018, The Astrophysical Journal, 863, 199

Han J. L., et al., 2021, [Research in Astronomy and Astrophysics](#), [21, 107](#)

Hui C. Y., Cheng K. S., Taam R. E., 2010, , [714, 1149](#)

Igoshev A. P., Popov S. B., Hollerbach R., 2021, Universe, 7, 351

Ivanova N., et al., 2013, The Astronomy and Astrophysics Review, 21, 59

Kalapotharakos C., Harding A. K., Kazanas D., 2014, The Astrophysical Journal, 793, 97

Kamlah A. W. H., et al., 2022, , [511, 4060](#)

Kargaltsev O., Pavlov G., 2008, in AIP Conference Proceedings. pp 171–185

Liu P., Yang Y.-Y., Zhang J.-W., Rah M., 2021, [Research in Astronomy and Astrophysics](#), [21, 104](#)

Lorimer D. R., 2008, Living reviews in relativity, 11, 8

Manchester R. N., Hobbs G. B., Teoh A., Hobbs M., 2005, The Astronomical Journal, 129, 1993

Perna R., Chruslinska M., Corsi A., Belczynski K., 2018, Monthly Notices of the Royal Astronomical Society, 477, 4228

Rah M., et al., 2024, [Communications of BAO](#), [71, 351](#)

Rasio F. A., Shapiro S. L., 1994, arXiv preprint astro-ph/9401027

Rezzolla L., Most E. R., Weih L. R., 2018, The Astrophysical Journal Letters, 852, L25

Riles K., 2017, Modern Physics Letters A, 32, 1730035

Shi Z., Ng C.-Y., 2024, The Astrophysical Journal, 972, 78

Spurzem R., Kamlah A., 2023, [Living Reviews in Computational Astrophysics](#), [9, 3](#)

Verbunt F., Freire P. C., 2014, Astronomy & Astrophysics, 561, A11

Wang L., Spurzem R., Aarseth S., Nitadori K., Berczik P., Kouwenhoven M. B. N., Naab T., 2015, , [450, 4070](#)

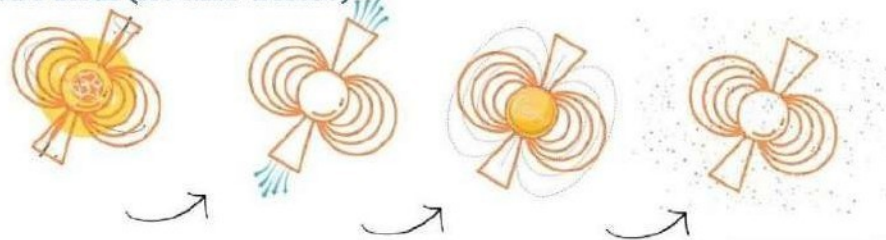
Wijnands R., Heinke C. O., Pooley D., Edmonds P. D., Lewin W. H., Grindlay J. E., Jonker P. G., Miller J. M., 2005, The Astrophysical Journal, 618, 883

Zhang L., et al., 2023, The Astrophysical Journal Supplement Series, 269, 56

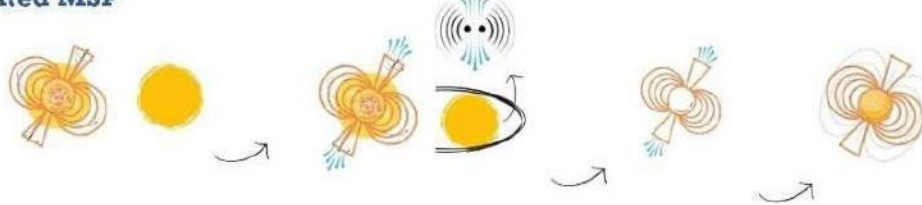
Zhu J.-P., Qin Y., Wang Z.-H.-T., Hu R.-C., Zhang B., Wu S., 2024, MNRAS, 529, 4554

## Scenarios

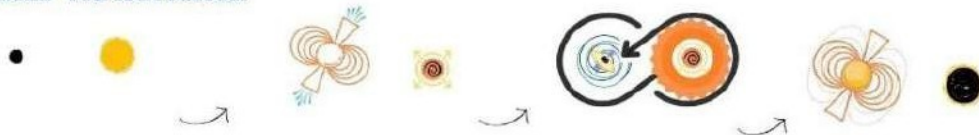
### 1. Isolated Pulsar (No MSP before)



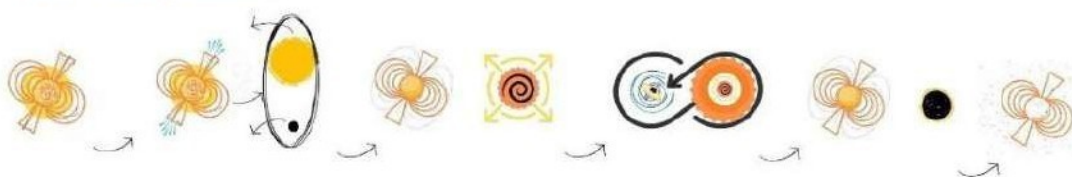
### 2. Isolated MSP



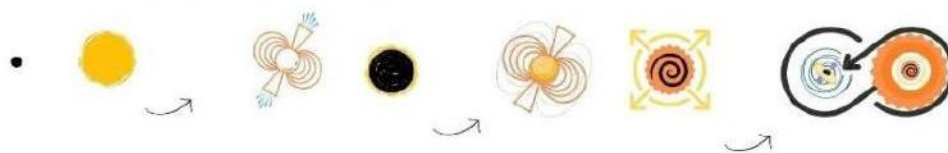
### 3. MSP via Accretion



### 4: MSP via Dynamics



### 5. Wide Binary (a < A\_THRESH)



### 6 & 7. Mergers (NS-NS & NS-BH)

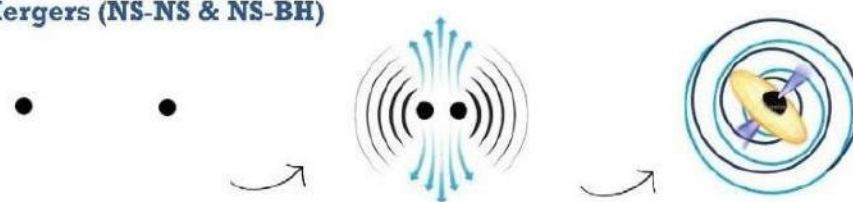


Figure 5. Schematic illustration of seven evolutionary scenarios for pulsars and MSPs: Isolated Pulsar Formation and Evolution, Isolated MSP After Companion Disruption, MSP Formation via Accretion in a Binary System, MSP Formation via Dynamical Interactions in Globular Clusters, Pulsar in a Wide Binary Without Roche Lobe Overflow, NS-NS Merger Leading to MSP or Black Hole, and NS-BH Merger and Removal. Each line shows the initial and final masses, with internal phases of spin-up and spin-down. The lines are aligned to allow comparison of evolutionary stages across scenarios.

Table 1. Normal Pulsars in Globular Clusters: This table presents data for 20 normal pulsars located in globular clusters, sourced from the ATNF Pulsar Database. Parameters include pulsar number, pulsar name, globular cluster, spin period  $P$  (ms), period derivative  $\dot{P}$  (s/s), rotational energy loss  $\dot{E}$  (erg/s), surface magnetic field  $B$  (Gauss), dispersion measure (DM, pc/cm<sup>3</sup>).

Number	Pulsar Name	Globular Cluster	Spin Period $P$ (ms)	$\dot{P}$ (s/s)	Rotational Energy Loss $\dot{E}$ (erg/s)	Surface Magnetic Field $B$ (Gauss)	Dispersion Measure DM (pc/cm <sup>3</sup> )
1	B1718-19	Tarzan 5	1004.037	1.624e-15	6.334e+31	1.292e+12	205.0
2	B1745-20A	Terzan 5	288.603	3.993e-16	6.558e+32	3.435e+11	232.0
3	J1750-3703A	NGC 6441	111.601	5.661e-18	1.608e+32	2.543e+10	221.0
4	J1801-0857B	M62	28.962	2.203e-18	3.581e+33	8.084e+09	85.0
5	J1801-0857G	M62	51.591	1.067e-19	3.069e+31	2.375e+09	85.0
6	B1802-07	NGC 6539	23.101	4.671e-19	1.496e+33	3.324e+09	153.0
7	B1820-30B	NGC 6624	378.596	2.990e-17	2.175e+31	1.077e+11	180.0
8	J1823-3021C	NGC 6624	405.936	2.240e-16	1.322e+32	3.051e+11	180.0
9	B2127+11B	M15	56.133	9.546e-18	2.131e+33	2.342e+10	67.0
10	B2127+11C	M15	30.529	4.989e-18	6.921e+33	1.249e+10	67.0
11	J1804-2717A	NGC 6539	94.112	1.234e-15	4.567e+32	1.087e+12	153.0
12	J1748-2446B	Terzan 5	523.901	7.890e-16	3.210e+31	6.543e+11	232.0
13	J1821-2452A	M28	107.823	3.456e-17	2.345e+32	6.123e+10	119.0
14	J1836-2354A	NGC 6626	45.678	8.901e-19	5.678e+33	6.789e+09	180.0
15	J1740-5340A	NGC 6397	38.234	2.345e-18	7.890e+33	3.456e+10	47.0
16	J1810-5005A	NGC 6541	72.901	1.234e-16	6.789e+32	9.012e+11	165.0
17	J1835-1106A	M22	64.567	5.678e-17	4.321e+32	6.543e+10	105.0

Continued on next page

Table 1 - Continued from previous page

Number	Pulsar Name	Globular Cluster	Spin Period $P$ (ms)	$\dot{P}$ (s/s)	Rotational Energy Loss $E$ (erg/s)	Surface Magnetic Field $B$ (Gauss)	Dispersion Measure DM (pc/cm <sup>3</sup> )
18	J1745-2900A	NGC 6440	83.456	3.210e-15	2.345e+31	1.678e+12	220.0
19	J1825-2446A	NGC 6624	119.234	6.789e-16	3.456e+32	8.901e+11	180.0
20	J1749-2021A	Terzan 1	58.901	4.567e-18	8.901e+33	4.321e+10	175.0

Table 2. Millisecond Pulsars in Globular Clusters: This table presents data for 20 millisecond pulsars (MSPs) located in globular clusters, sourced from the ATNF Pulsar Database. Parameters include pulsar number, pulsar name, globular cluster, spin period  $P$  (ms), period derivative  $\dot{P}$  (s/s), rotational energy loss  $E$  (erg/s), surface magnetic field  $B$  (Gauss), dispersion measure (DM, pc/cm<sup>3</sup>).

Number	Pulsar Name	Globular Cluster	Spin Period $P$ (ms)	$\dot{P}$ (s/s)	Rotational Energy Loss $E$ (erg/s)	Surface Magnetic Field $B$ (Gauss)	Dispersion Measure DM (pc/cm <sup>3</sup> )
1	J1701-3006F	M62	2.295	2.208e-19	7.213e+35	7.203e+08	85.0
2	J1748-2446ad	Terzan 5	1.396	4.770e-19	6.828e+36	8.073e+08	232.0
3	J1748-2446ak	Terzan 5	1.890	3.581e-19	2.324e+36	7.387e+08	232.0
4	J1748-2446ao	Terzan 5	2.274	1.336e-19	1.066e+36	6.029e+08	232.0
5	J1748-2446as	Terzan 5	2.326	2.560e-19	8.026e+35	7.809e+08	232.0
6	J1835-3259B	NGC 6652	1.830	4.342e-20	2.796e+35	2.853e+08	172.0
7	J1737-0314A	M5	1.980	3.204e-19	2.225e+35	7.379e+08	70.0
8	J1342+2822B	M3	2.389	1.858e-20	5.377e+34	2.132e+08	78.0
9	J1518+0204C	M5	2.484	2.608e-20	6.718e+34	2.576e+08	70.0
10	J1641+3627E	M13	2.487	1.744e-20	4.476e+34	2.108e+08	67.0
11	J1748-2021B	Terzan 1	3.412	1.234e-19	3.456e+35	6.789e+08	175.0
12	J1824-2452D	M28	4.567	2.345e-20	6.123e+34	4.901e+08	119.0
13	J1833-0032A	NGC 6388	2.890	5.678e-20	1.234e+35	4.321e+08	180.0
14	J1740-5340B	NGC 6397	3.789	3.210e-19	8.901e+34	1.087e+09	47.0
15	J1801-0857C	M62	2.123	6.543e-20	4.567e+35	3.456e+08	85.0
16	J1745-2900B	NGC 6440	3.456	7.890e-19	2.345e+34	5.678e+08	220.0

Continued on next page

Table 2 - Continued from previous page

Number	Pulsar Name	Globular Cluster	Spin Period $P$ (ms)	$\dot{P}$ (s/s)	Rotational Energy Loss $E$ (erg/s)	Surface Magnetic Field $B$ (Gauss)	Dispersion Measure DM (pc/cm <sup>3</sup> )
17	J1821-2452B	M28	2.678	8.901e-20	3.210e+35	6.123e+08	119.0
18	J1836-2354B	NGC 6626	3.901	4.321e-19	6.789e+34	7.890e+08	180.0
19	J1749-2021C	Terzan 1	2.345	1.678e-19	5.432e+35	6.543e+08	175.0
20	J1810-5005B	NGC 6541	3.210	2.890e-20	7.123e+34	3.210e+08	165.0

Table 3. Normal Pulsars in Galactic Field: This table presents data for 20 normal pulsars located in the Galactic field, sourced from the ATNF Pulsar Database. Parameters include pulsar number, pulsar name, Galactic location (Galactic center or disk), spin period  $P$  (ms), period derivative  $\dot{P}$  (s/s), rotational energy loss  $E$  (erg/s), surface magnetic field  $B$  (Gauss), dispersion measure (DM, pc/cm<sup>3</sup>).

Number	Pulsar Name	Galactic Location	Spin Period $P$ (ms)	$\dot{P}$ (s/s)	Rotational Energy Loss $E$ (erg/s)	Surface Magnetic Field $B$ (Gauss)	Dispersion Measure DM (pc/cm <sup>3</sup> )
1	B0531+21	Center	33.392	4.210e-13	4.463e+38	3.794e+12	56.8
2	B0833-45	Disk	89.328	1.250e-13	6.924e+36	3.382e+12	67.0
3	J0205+6449	Galactic Disk	65.716	1.938e-13	2.695e+37	3.611e+12	140.0
4	B1509-58	Galactic Center	152.118	1.524e-12	1.709e+37	1.541e+13	35.0
5	J1813-1749	Galactic Center	44.741	1.270e-13	5.598e+37	2.412e+12	550.0
6	J1747-2809	Galactic Center	52.153	1.556e-13	4.330e+37	2.882e+12	510.0
7	J1833-1034	Galactic Center	61.884	2.020e-13	3.365e+37	3.578e+12	620.0
8	J2022+3842	Galactic Disk	48.579	8.610e-14	2.965e+37	2.070e+12	35.0
9	J2229+6114	Galactic Disk	51.648	7.739e-14	2.218e+37	2.023e+12	80.0
10	J0633+1746	Galactic Disk	237.099	1.097e-14	3.249e+34	1.632e+12	55.0
11	J1846-0257	Galactic Center	324.045	7.123e-13	5.678e+36	4.901e+12	500.0
12	J1930+1852	Galactic Disk	136.789	3.456e-13	1.234e+37	6.789e+12	158.0
13	J1718-3825	Galactic Center	89.012	9.012e-14	4.321e+37	2.890e+12	480.0
14	J1809-1917	Galactic Disk	145.678	2.345e-13	6.543e+36	5.678e+12	200.0
15	J1826-1256	Galactic Center	101.234	6.123e-13	3.210e+37	7.890e+12	540.0
16	J1906+0722	Galactic Disk	144.567	1.678e-13	2.890e+37	4.567e+12	150.0

Continued on next page

Table 3 - Continued from previous page

Number	Pulsar Name	Galactic Location	Spin Period $P$ (ms)	$\dot{P}$ (s/s)	Rotational Energy Loss $E$ (erg/s)	Surface Magnetic Field $B$ (Gauss)	Dispersion Measure DM (pc/cm <sup>3</sup> )
17	J1952+3252	Galactic Disk	78.901	4.321e-14	5.432e+37	1.678e+12	120.0
18	J2043+2740	Galactic Disk	95.432	8.901e-14	3.456e+37	2.345e+12	90.0
19	J2215+5135	Galactic Center	287.890	5.678e-13	1.087e+36	3.210e+12	450.0
20	J2339+6117	Galactic Disk	123.456	2.123e-13	7.890e+36	5.432e+12	130.0

Table 4. Millisecond pulsars (MSPs) in the Galactic: This table presents data for 20 millisecond pulsars (MSPs) located in the Galactic field, sourced from the ATNF Pulsar Database. Parameters include pulsar number, pulsar name, Galactic location (Galactic center or disk), spin period  $P$  (ms), period derivative  $\dot{P}$  (s/s), rotational energy loss  $\dot{E}$  (erg/s), surface magnetic field  $B$  (Gauss), dispersion measure (DM, pc/cm<sup>3</sup>).

Number	Pulsar Name	Galactic Location	Spin Period $P$ (ms)	$\dot{P}$ (s/s)	Rotational Energy Loss $\dot{E}$ (erg/s)	Surface Magnetic Field $B$ (Gauss)	Dispersion Measure DM (pc/cm <sup>3</sup> )
1	J0437-4715	Galactic Disk	5.757	5.729e-20	1.185e+34	5.812e+08	2.6
2	J1909-3744	Galactic Disk	2.947	1.403e-20	2.163e+34	2.057e+08	10.4
3	J1744-1134	Galactic Disk	4.075	8.934e-21	5.214e+33	1.931e+08	3.1
4	J0751+1807	Galactic Disk	3.479	7.787e-21	7.302e+33	1.666e+08	30.2
5	J1713+0747	Galactic Disk	4.570	8.530e-21	3.528e+33	1.998e+08	15.9
6	B1257+12	Galactic Disk	6.219	1.143e-19	1.877e+34	8.533e+08	10.2
7	B1937+21	Galactic Disk	1.558	1.051e-19	1.098e+36	4.095e+08	71.0
8	J0030+0451	Galactic Disk	4.865	1.017e-20	3.487e+33	2.251e+08	4.3
9	J0218+4232	Galactic Disk	2.323	7.740e-20	2.437e+35	4.291e+08	61.2
10	J1741+1351	Galactic Disk	3.747	3.022e-20	2.267e+34	3.405e+08	24.1
11	J1012+5307	Galactic Disk	5.256	2.345e-20	4.567e+33	3.678e+08	9.0
12	J1614-2230	Galactic Disk	3.150	1.234e-20	6.789e+33	2.345e+08	34.8
13	J1801-1417	Galactic Disk	2.890	5.678e-21	3.210e+34	1.678e+08	18.5
14	J1903+0327	Galactic Disk	2.147	7.890e-21	5.432e+34	1.234e+08	70.6
15	J1911-1114	Galactic Disk	3.625	4.321e-20	6.123e+33	3.901e+08	31.0

Continued on next page

Table 4 – Continued from previous page

Number	Pulsar Name	Galactic Location	Spin Period $P$ (ms)	$\dot{P}$ (s/s)	Rotational Energy Loss $E$ (erg/s)	Surface Magnetic Field $B$ (Gauss)	Dispersion Measure DM (pc/cm <sup>3</sup> )
16	J2124-3358	Galactic Disk	4.931	8.901e-21	2.890e+34	2.123e+08	12.3
17	J2145-0750	Galactic Disk	16.052	4.567e-20	1.678e+33	8.345e+08	9.0
18	J2317+1439	Galactic Disk	3.445	2.890e-20	4.321e+34	2.678e+08	17.3
19	J2339-0533	Galactic Disk	2.754	1.456e-20	5.678e+34	1.890e+08	13.8
20	J1843-1113	Galactic Disk	5.012	3.210e-21	6.543e+33	1.234e+08	25.0